ADVANCED FUNCTIONAL MATERIALS
www.afm-journal.de

Understanding Local and Macroscopic Electron Mobilities in the Fullerene Network of Conjugated Polymer-based Solar Cells: Time-Resolved Microwave Conductivity and Theory

Jordan C. Aguirre, Christopher Arntsen, Samuel Hernandez, Rachel Huber, Alexandre M. Nardes, Merissa Halim, Daniel Kilbride, Yves Rubin, Sarah H. Tolbert, Nikos Kopidakis, Benjamin J. Schwartz, and Daniel Neuhauser*

The efficiency of bulk heterojunction (BHJ) organic photovoltaics is sensitive to the morphology of the fullerene network that transports electrons through the device. This sensitivity makes it difficult to distinguish the contrasting roles of local electron mobility (how easily electrons can transfer between neighboring fullerene molecules) and macroscopic electron mobility (how well-connected is the fullerene network on device length scales) in solar cell performance. In this work, a combination of density functional theory (DFT) calculations, flash-photolysis time-resolved microwave conductivity (TRMC) experiments, and space-charge-limit current (SCLC) mobility estimates are used to examine the roles of local and macroscopic electron mobility in conjugated polymer/fullerene BHJ photovoltaics. The local mobility of different pentaaryl fullerene derivatives (so-called 'shuttlecock' molecules) is similar, so that differences in solar cell efficiency and SCLC mobilities result directly from the different propensities of these molecules to self-assemble on macroscopic length scales. These experiments and calculations also demonstrate that the local mobility of phenyl-C_{60} butyl methyl ester (PCBM) is an order of magnitude higher than that of other fullerene derivatives, explaining why PCBM has been the acceptor of choice for conjugated polymer BHJ devices even though it does not form an optimal macroscopic network. The DFT calculations indicate that PCBM's superior local mobility comes from the near-spherical nature of its molecular orbitals, which allow strong electronic coupling between adjacent molecules. In combination, DFT and TRMC techniques provide a tool for screening new fullerene derivatives for good local mobility when designing new molecules that can improve on the macroscopic electron mobility offered by PCBM.

1. Introduction

There are a number of factors that can limit the power conversion efficiency (PCE) of organic photovoltaics, including the efficiency of exciton generation and separation,[1–4] the mobilities of the subsequently generated electrons and holes,[5–8] and the nanometer-scale morphology of the bulk heterojunction (BHJ) network that determines how easily carriers can reach the electrodes or recombine.[9–14] The importance of the network morphology can be seen in the fact that a number of organic electron donors and acceptors with seemingly optimally matched energy levels produce poorly performing solar cells because they have an improper degree of phase segregation when blended together.[15,16] Because of this, there has been a great deal of effort to use processing conditions to control BHJ morphology, including the use of solvent additives,[17–19] post-fabrication thermal annealing,[20–22] and sequential deposition of the donor and acceptor layers.[23–30] All of these techniques greatly increase the parameter space for optimizing power conversion efficiency, which is detrimental when most of the progress in increasing PCE for a given set of materials is made via exploring this parameter space through trial-and-error.

In previous work, we developed a method to control the nanometer-scale morphology of the BHJ network in polymer/fullerene photovoltaics using pentaaryl-substituted fullerenes that self-assemble into one-dimensional stacks.[31–33] The idea is that pentaaryl substitution creates fullerene molecules with a self-complementary shape that promotes stacking; because of their shape, we (and others[34–37]) have referred to this class of fullerene derivatives as 'shuttlecocks' (SCs). When exploring the behavior of SCs in photovoltaic blends with poly(3-hexylthiophene) (P3HT), we found that the SCs that formed 1-dimensional stacks had significantly improved photovoltaic performance compared with nearly identical fullerenes that had *meta*

J. C. Aguirre, C. Arntsen, S. Hernandez, R. Huber, M. Halim, D. Kilbride, Prof. Y. Rubin, Prof. S. H. Tolbert, Prof. B. J. Schwartz, Prof. D. Neuhauser
Department of Chemistry and Biochemistry
University of California
Los Angeles, California, 90095-1569, USA
E-mail: schwartz@chem.ucla.edu
Dr. A. M. Nardes, Dr. N. Kopidakis
Chemical and Nanoscience Center National
Renewable Energy Laboratory
15013 Denver West Parkway, Golden, CO 80401, USA

DOI: 10.1002/adfm.201301757

substitution on the SC 'feathers' that inhibited the ability to stack.[31] Subsequently, we worked to control the propensity for stacking by varying the size of alkyl substituents in the *para* position of the SC feathers. We found using X-ray diffraction and atomic force microscopy that varying the functionalization of the pentaaryl feather substituents by a single methyl group lead to dramatic differences in nanoscale morphology in blends with P3HT.[32] This is because SCs with shorter alkyl feather substituents tend to stack less easily than those with longer substituents [33]; non-stacking SCs prefer to phase separate from the donor polymer, whereas the more self-assembling fullerene derivatives preserve the desired blended nanoscale architecture.[32] As a result, the PCE of devices based on fullerene self-assembly was improved due both to enhanced charge separation and an increase in electron mobility throughout the assembled fullerene network.[31]

Even though we were able to demonstrate that self-assembly produces a fullerene network that leads to improved photovoltaic performance, the power conversion efficiency of devices based on SCs fell well short of those utilizing the well-studied [6,6]-phenyl-C_{60}-butyric acid methyl ester (PCBM) fullerene derivative as the electron acceptor. Since PCBM does not self-assemble into one-dimensional stacks, the fact that PCBM devices perform better than SC-based devices indicates that network formation is not the only factor contributing to electron mobility in a BHJ device. This suggests that there are (at least) two length scales over which electron mobility is determined in the fullerene network: the macroscopic length scale (i.e., the active layer thickness) over which the electrons must move to be extracted from the device, and a shorter-ranged molecular length scale over which the probability for an electron to hop from one fullerene molecule to the adjacent one is determined. Although a high local electron mobility does not guarantee high macroscopic mobility (since macroscopic mobility can be limited by grain boundaries, the fractal nature of the network etc.), poor local mobility clearly limits the macroscopic performance of a device. It is therefore plausible that molecules like PCBM have local electron mobilities that are so high compared to those of SC derivatives that SC-based devices do not perform as well PCBM-based devices, even though SCs form a better macroscopic network.

Although there are many methods for measuring the macroscopic mobility of the carriers in organic photovoltaics, it is less clear how to measure the role that local mobility plays in device performance. Thus, in this paper we aim to ascertain how device-wide network formation and local molecular arrangements collectively determine electron extraction from polymer/fullerene solar cells. We start by developing a density functional theory (DFT)-based computational technique to examine the electronic coupling between adjacent fullerene molecules, providing a theoretical estimate of the 'local' electron mobility. To verify that our calculation protocol makes physical sense, we then turn to time-resolved microwave conductivity (TRMC) experiments that directly measure local conductivities in P3HT/fullerene blend films. We find that the experimentally-measured TRMC local mobilities correlate well with the theoretical predictions. Taken together, the two techniques are able to explain general features of organic photovoltaic device performance, including why PCBM is the acceptor of choice for most polymer-based solar cells even though it does not form the best macroscopic network. The fact that the theoretical predictions are validated by experiment also indicates that we can use such calculations to determine 'design rules' for new fullerene acceptors that could potentially outperform PCBM. And perhaps more importantly, the fact that most fullerene acceptors (including PCBM) do not form networks that simultaneously optimize both the local and macroscopic electron mobilities indicates that there is still significant room for improvement in the fullerene component of polymer/fullerene solar cells.

2. Results and Discussion

2.1. Electronic Coupling Determined through Density Functional Theory Calculations

In polymer/fullerene solar cells, electron mobility at the local level consists of charge transfer between neighboring fullerene acceptors. To understand how the local rate of electron transfer varies between different fullerene derivatives, we developed a DFT-based protocol to calculate the electronic coupling between pairs of fullerene molecules in a variety of geometries. The electron transfer problem we consider consists of moving charge between two fullerene molecules, which we label left (L) and right (R):

$$L^- + R \rightarrow L + R^- \tag{1}$$

The fundamental quantity of interest is the electronic coupling γ between the L and R molecules, which has the form:[39,40]

$$\gamma(L \rightarrow R) = |\langle \Psi_L | H | \Psi_R \rangle| \tag{2}$$

where H is the total Hamiltonian and Ψ_i is the localized wavefunction of the transferred electron on molecule i (i.e., the LUMO of the neutral molecule). In our case, the Hamiltonian and wavefunctions are calculated with DFT, which has been shown to give good accuracy within the Marcus theory framework,[41–46] using the B3LYP functional and STO-3G basis set. Direct calculation of γ, however, can be problematic. This is because if the effects of the environment are ignored, the electron can be artificially localized on an individual molecule due to asymmetry in the system. To overcome this problem, when calculating γ we apply an electric field to delocalize the excited states across the two-molecule system. This is because in a real BHJ system, each fullerene molecule sees, on average, an identical chemical environment; our application of an external field in effect 'equilibrates' the system and allows the electron to delocalize between the two molecules the way it would in the bulk system. This means that with the application of the field, the LUMO and LUMO+1 orbitals are not localized on the same molecule, so we can easily calculate γ from the energy splitting between these two orbitals. More specifically, in a two-level system, the coupling between the two levels is equal to the half-splitting of the levels in the diagonal basis. Therefore, we rotated the two-level Hamiltonian into the diabatic basis, and found the coupling simply from the off-diagonal elements; the details of how we performed these calculations are described in the Supporting Information (SI).

DOI: 10.1002/adfm.201301757

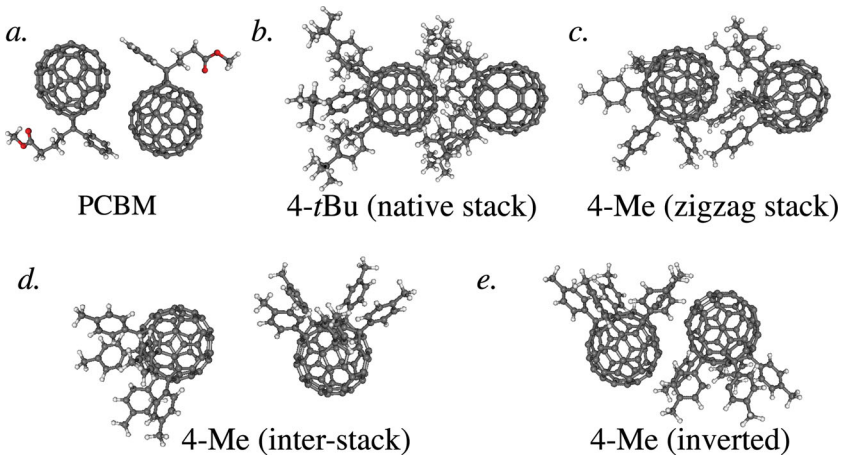

Figure 1. Chemical structures of the fullerene derivatives considered in this work and the geometries of the fullerene pairs used in our DFT calculations. a) PCBM, taken from the crystal structure in Ref. [38]; b) the 4-*t*Bu shuttlecock molecule in its stacked orientation, taken from the crystal structure in Ref. [33]; c) the 4-Me shuttlecock in its native crystal structure, taken from Ref. [33]: note the 4-Me molecules crystallize in a 'zigzag stack' motif rather than the linear 'ball-in-cup' exhibited by 4-*t*Bu; d) the 4-Me molecule in its interstack geometry over which we varied the separation distance of the individual molecules; e) 4-Me molecules in a head-to-tail ('inverted stack') geometry similar to that of PCBM molecules, taken from Ref. [33]. The red color in PCBM denotes oxygen atoms; none of the other molecules contain any hetero-atoms. See SI for details.

To tie in with our previous work on self-assembling fullerenes, we started by examining the coupling between two SC molecules, 6,9,12,15,18-pentakis(4-*tert*-butylphenyl)-1-hydro[60]fullerene (4-*t*Bu) and 6,9,12,15,18-pentakis(4-methylphenyl)-1-hydro[60]fullerene (4-Me). We chose these two SC fullerenes because they present a sharp contrast in their ability to self-assemble. Previously, we found that 4-*t*Bu was a 'universal stacker', assembling into one-dimensional stacks when crystallized from essentially every solvent we explored,[33] which in turn lead to the best solar cell performance of all the SC fullerenes we examined.[32] In contrast, the 4-Me molecule, which is electronically identical to 4-*t*Bu, appeared to show little propensity for columnar self-assembly,[33] which resulted in poor device performance.[32] Finally, to understand how local mobility among the fullerenes influences overall device performance, we also elected to examine coupling between molecules of the well-studied PCBM. The chemical structures of the 4-*t*Bu, 4-Me and PCBM fullerene derivatives, as well as the geometries we used for calculating the electronic coupling between pairs of these molecules, are shown in **Figure 1** (and the precise coordinates used in our calculations are given in the SI).

Although we do not know the distribution of geometries of pairs of fullerene molecules in a working BHJ device, it seems reasonable that on molecular length scales, the spatial relationship between adjacent fullerene molecules should be similar to that in single crystals. Thus, we chose geometries for our calculations for the 4-Me and 4-*t*Bu derivatives from the crystal structures found in our previous work.[33] For the electronic coupling in 4-*t*Bu dimers, we considered only the linearly stacked orientation found in the crystals derived from most different organic solvents (Figure 1b). For pairs of 4-Me molecules, we calculated the electronic coupling in a 'zigzag stack' geometry taken from crystals formed in toluene (Figure 1c) and a head-to-tail 'inverted' geometry taken from crystals formed in methanol (Figure 1*e*). For completeness, we also calculated the coupling between 4-Me dimers at their 'interstack' geometry (Figure 1d). In the native crystal, the interstack 4-Me orientation contains interstitial solvent molecules, which prevent the 4-Me molecules from residing close together. Since there likely is not any solvent present between fullerene molecules in a BHJ device, to calculate the electron transfer probability between 4-Me molecules in this orientation, we eliminated the solvent from the crystal structure and repeated the calculation over intermolecular distances ranging from 11.2 Å to 15.2 Å center-to-center fullerene separation (the lower end of this range is limited by van der Waals contact between the 4-Me molecules, while the upper end is what is found in the native crystal with interstitial solvent molecules). Finally, for the electronic coupling between PCBM molecules (Figure 1a), we took the geometry from the PCBM crystal structure in Reference [38].

Using these geometries and our DFT-based method, which is outlined above and in the SI, we calculated the electronic coupling between multiple pairs of fullerene molecules and obtained the results summarized in **Table 1**. For the SC fullerene derivatives, we find that both the 4-Me and 4-*t*Bu molecular pairs have essentially the same electronic coupling (within 10%) when placed in their respective 'stacking' orientations; this result makes sense given that 4-Me and 4-*t*Bu have an identical electronic structure, so the overlap of their LUMOs is about the same when adjacent molecules are forced to have similar geometries. When the SC molecules are not in the desired stacked geometry, the electronic coupling varied strongly (roughly exponentially) with the average distance between the fullerene balls. At the closest possible non-stacked distance (limited by steric hindrance of the alkyl substituents), the coupling is actually slightly higher than that in the stacked geometry. Thus, even though we do not know the precise geometry between neighboring SC fullerene molecules in BHJ devices, we can conclude that as long as

Table 1. Calculated electron couplings for fullerene molecular dimers with the geometries shown in Figure 1. Couplings were calculated using the DFT-based methods outlined in the SI.

Molecule	Center-to-Center Distance [Å]	Coupling [eV]
4-*t*Bu (native stack)	10.8	2.95×10^{-4}
4-Me (zigzag stack)	10.9	2.64×10^{-4}
4-Me (interstack)	11.2–15.2	$1.75 \times 10^{-7} - 4.15 \times 10^{-4}$
4-Me (inverted)	9.9	1.45×10^{-3}
PCBM	10.2	1.00×10^{-2}

these molecules stay in close van der Waals contact, the electronic coupling of the pentaaryl fullerenes is comparable in any geometry, lying in the range of 10^{-4} to low 10^{-3} eV.

The fact that the molecular length-scale coupling between pentaaryl fullerenes is similar in nearly every geometry has important implications for solar cells built from these materials. Since the local coupling of these molecules is the same because the molecules have identical electronic structure (i.e., identical HOMO and LUMO levels with similar orbitals), the large differences in device performance we observed for these two molecules[32] must be the result of differences in the macroscopic geometry of the fullerene network. This makes sense given that 4-*t*Bu shuttlecocks self-assemble into long stacks, creating a much better macroscopic fullerene network throughout the active layer than 4-Me molecules, which phase-segregate from the polymer into unconnected islands.[32] Thus, self-assembly can indeed improve the macroscopic network of polymer-fullerene BHJ solar cells, as we demonstrated experimentally in previous work.[31]

Also shown in Table 1 are the results of the electronic coupling calculation for a pair of PCBM molecules. We find that the electronic coupling between neighboring PCBM molecules is roughly two orders of magnitude larger than the average coupling between the SC fullerenes. This explains why devices built from the SC fullerenes perform so much more poorly than devices built with PCBM, even though the assembled macroscopic 4-*t*Bu fullerene network is likely better than the random PCBM network: electrons are simply more efficiently moved between PCBM molecules than between SC molecules.

Why is the electronic coupling so much higher between PCBM molecules than other fullerenes? For PCBM, the LUMO and LUMO+1 orbitals are highly delocalized around the molecule in a nearly spherically symmetric fashion, as shown in **Figure 2**a. This allows for greater orbital overlap between neighboring molecules no matter what their relative geometry. In contrast, the frontier orbitals of the 4-*t*Bu and 4-Me shuttlecocks are fairly localized, with the electron density avoiding the regions near and inside the pentaaryl feathers, as illustrated in Figure 2b. This means that when the SC molecules are stacked, there is relatively poor overlap of the orbitals on the neighboring molecules: the electron density on the ball of one SC has little overlap with the electron density in the 'bowl' of the next SC in the stack. The non-spherical orbital distribution of the SCs also explains why the electronic coupling in the non-stacking direction is roughly equivalent to that in the stacked direction, since the electronic overlap in this geometry is equally as poor.

In summary, our calculations suggest that even though pentaaryl fullerenes self-assemble into excellent macroscopic BHJ networks, the electron mobility of these compounds is limited at the local, molecular length scale. Moreover, our calculations also suggest that PCBM is a champion electron acceptor for organic photovoltaics because the electron transfer rate between PCBM molecules is not only outstanding, but also is roughly independent of the molecular geometry. In the next section, we turn to time-resolved microwave conductivity (TRMC) to provide an experimental verification of these ideas concerning local mobility. But most importantly, what these calculations tell us is that if one wishes to create new self-assembling fullerene acceptors, a key design goal must be to have strong orbital overlap between adjacent fullerenes.

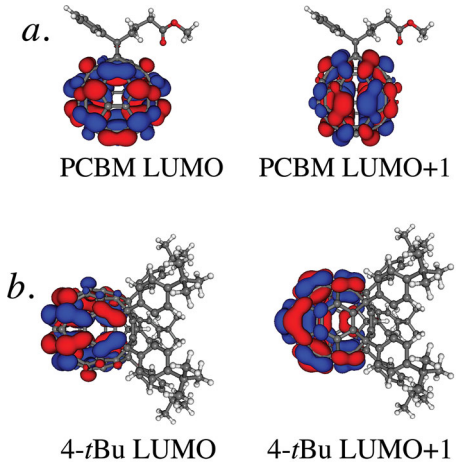

Figure 2. Kohn-Sham orbitals from our DFT calculations corresponding to the LUMO and LUMO+1 of the isolated fullerene molecules: a) PCBM, and b) 4-*t*Bu. The orbitals were calculated using the B3LYP functional and STO-3G basis set (see SI for details).

2.2. Local Electron Mobility Determined through Time-Resolved Microwave Conductivity

Although there are numerous methods for estimating the mobility of the carriers in organic photovoltaic devices (e.g., fitting space-charge-limited current models to single-carrier diodes built from the active materials,[47] building field effect transistors from the materials,[48] various transient photovoltage and photocurrent experiments,[49–52] etc.) all of these methods measure carrier motion only at the macroscopic, device length scale. Moreover, most of these methods also are sensitive to the nature of the contacts between the electrodes and the active material(s). To experimentally probe the local mobility of photogenerated carriers, it is necessary to turn to an electrodeless pump-probe method. Flash photolysis TRMC provides exactly such a method,[53,54] and thus offers the perfect testbed for comparing our calculations in the previous section to an experimental measure of local electron mobility; the TRMC technique has been used previously to comparing local and network-wide hole mobility in samples of P3HT.[55]

The flash photolysis TRMC technique measures the time-dependent change of the microwave power in a cavity that contains the sample following the photogeneration of charges in that sample. The microwave power absorbed is directly related to the photoconductance of the sample, which is proportional to the yield of photogenerated carriers per photon absorbed (φ) and the (sum of the) high-frequency (local) effective mobility ($\Sigma\mu$) of those carriers.[56] For TRMC experiments, the measured photoconductance peak (ΔG_{peak}) is given by:

$$\Delta G_{peak} = \beta q_e d(n\mu_e + p\mu_h) \quad (3)$$

Adv. Funct. Mater. **2013**,
DOI: 10.1002/adfm.201301757

where β is the ratio of the interior dimensions of the microwave waveguide (2.2 for our experimental set-up), qe is electronic charge, d is the sample thickness, and n and p are the density of the photogenerated electrons and holes, respectively. Since it is difficult to measure the densities of the individual carriers, Equation (3) is usually rewritten as:

$$\Delta G_{peak} = \beta q_e I_0 F_A \varphi(\mu_e + \mu_h) \quad (4)$$

where I_0 is the incident flux of photons used to excite the sample to create photoconducting carriers, and F_A is the fraction of those photons that are absorbed, given by $F_A = 1 - 10^{-OD}$, where OD is the optical density of the sample at the excitation wavelength. Since β, q_e, I_0, and F_A are all easily measured (as described in the SI), the TRMC experiment directly yields the product of the yield (or quantum efficiency) of free carriers per absorbed photon (φ) and the sum of their mobilities, $\mu_e + \mu_h$, or $\varphi\Sigma\mu$. Details of how we perform our TRMC measurements are described in the Supporting Information.

To understand the nature of the local mobility for the molecules we examined theoretically in the previous section, we prepared BHJ films of P3HT with both the 4-Me and 4-*t*Bu shuttlecock molecules and with PCBM. For some samples, we prepared the BHJ blends in a manner identical to our previous work studying photovoltaic devices made from these materials using equimolar ratios of PCBM, 4-*t*Bu, and 4-Me (polymer:fullerene weight ratios of 1:0.8, 1:0.45 and 1:0.35, respectively);[32] for others, we used very low loadings of the different fullerenes (P3HT:fullerene weight ratios of 1:0.0015 and 1:0.0013 for 4-*t*Bu and 4-Me respectively), as described in the SI. **Figure 3** shows how the $\varphi\Sigma\mu$ product—the carrier yield times the effective mobility—varies in all of our samples as a function of absorbed photon flux. Although Equation (4) predicts a linear relationship between ΔG_{peak} and $I_0 F_A$, there is a sublinear relationship at higher light intensities observed in Figure 3 that is due to exciton-charge annihilation, which causes the carrier concentration (φ) to drop at high excitation intensities.[56] Since our experimental apparatus cannot measure the absorbed microwave power at intensities low enough to be entirely in the linear regime, we fit the data using the formalism described in the SI (see Equation S3) to extract an extrapolated low-light-intensity value for $\varphi\Sigma\mu$. These extrapolated values are summarized in **Table 2**.

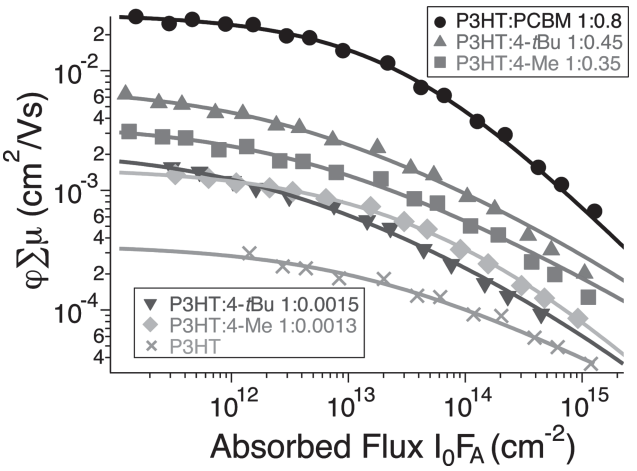

Figure 3. The dependence of $\varphi\Sigma\mu$, calculated from the measured TRMC photoconductance via Equation 1, on absorbed photon flux (I_0 F_A) for pure P3HT and blends with different fullerenes. The solid curves are fits to Equation S3 in the SI.

The first thing that is clear from Figure 3 and Table 2 is that the BHJ samples with low loadings of fullerene show increased photoconductivity compared to pure P3HT. This results from the fact that the presence of even a limited number of fullerene acceptors greatly increases the number of photogenerated carriers relative to pure P3HT.[57,58] We find that at these low acceptor loadings, the photoconductance of both the 4-*t*Bu and 4-Me pentaaryl fullerenes are fairly similar to each other, although different from what has been measured previously for low concentrations of PCBM in P3HT.[57] Since we expect the mobility of the holes on P3HT to be independent of the choice of fullerene at such low concentrations and there to be little electron mobility when the fullerenes are isolated at such low concentrations, most of the difference in photoconductance we measure must result from differences in the number of photogenerated carriers when different fullerenes are used. We will use this difference in carrier yields for different fullerenes, in combination with photoluminescence quenching experiments, to extract the local mobility of electrons among the network of different fullerenes present at device loadings, as described further below.

Table 2. Summary of low-light-intensity photoconductance and average exciton lifetimes in different P3HT:fullerene blends.

Sample	$\varphi\Sigma\mu$ [a)]	Exciton Lifetime[b)]	PL Quenching Carrier Yield	TRMC Carrier Yield	ns/ps Yield Ratio	'Corrected' ns Yield	Hole mobility[c)]	Calculated electron mobility[c)]
P3HT:4-Me 1:0.0013	0.15	121	41%	11%	0.26	NA	1.4	0
P3HT:4-*t*Bu 1:0.0015	0.21	128	37%	15%	0.40	NA	1.4	0
P3HT:4-Me 1:0.35	0.30	78	62%	NA	0.26[d)]	16%	1.4	0.44
P3HT:4-*t*Bu 1:0.45	0.60	43	79%	NA	0.40[d)]	32%	1.4	0.49
P3HT:PCBM 1:0.8	2.79	47	77%	NA	NA	77%	1.4	2.2
Pure P3HT	0.02	204	NA	1.4%	NA	NA	1.4	NA[a)]

[a)]10^{-2} cm^2/Vs; b)ps; [c)] 10^{-2} cm^2/Vs $\varphi\Sigma\mu$ values were determined via Equation 1 from the TRMC measurements in Figure 3 (see SI). Exciton lifetimes determined from deconvoluting the PL decay data in Figure 4 (see SI); [d)]Yield ratio values taken from samples with low fullerene loading.

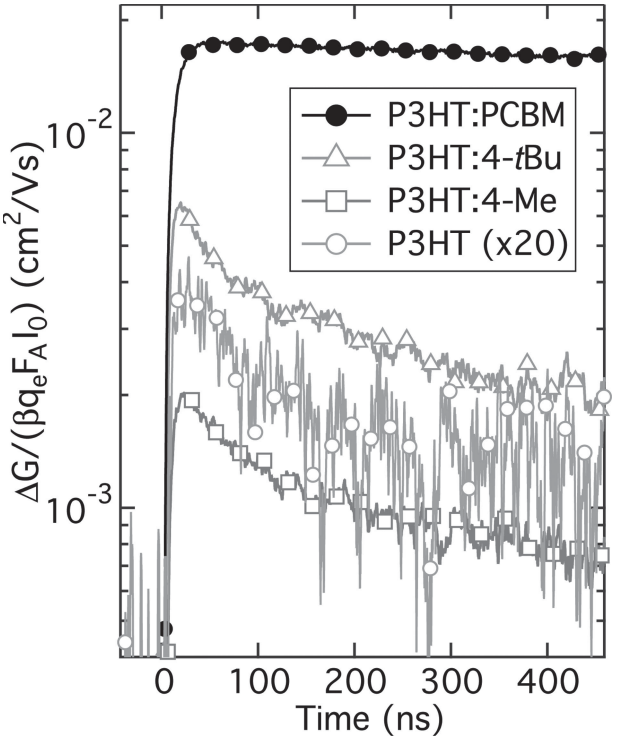

Figure 4. TRMC photoconductance transients (normalized for absorbed photon flux and physical constants, see Equation (4)) for P3HT-based samples at device loadings with different fullerenes. The photoexcitation wavelength was 500 nm, and the data shown are for an absorbed photon flux of 10^{12} cm^{-2}, which corresponds to a fluence of 0.56 mJ/cm^2. The results were similar, however, at all photon fluxes examined in this work.

Figure 3 and Table 2 also show that increasing the concentration of fullerenes in P3HT blend films to that present in typical photovoltaic devices further increases the photoconductance signal. Moreover, blend films containing 4-*t*Bu show a higher photoconductance than samples utilizing 4-Me as the acceptor, and neither of the SC fullerenes gives a photoconductance as high as that in P3HT:PCBM blends. To understand where these differences in photoconductance come from at high loadings, we examined the photoconductance decay profiles of the different blends, which are shown in **Figure** 4. The difference we observe between the photoconductance decay profiles of the P3HT:PCBM blend and that of pure P3HT has been attributed in previous work to differences in the type of carrier that dominates the TRMC signal: the mobility of electrons in PCBM is higher than that of holes in P3HT, hence the electrons dominate the photoconductance in the P3HT:PCBM sample.[57] The slow decay of ΔG observed in this case is attributed to slow bimolecular recombination at low excitation intensities.[57] In contrast, the photoconductance decays of the P3HT:SC blends are similar to those of the pure P3HT sample, indicating that for these blends the dominant ΔG term arises from the holes in P3HT, which have distinctly different dynamics than the electrons.[57] Although Figure 4 only shows representative transients at a specific excitation intensity, this observation holds at all the light intensities we used in this work. We therefore conclude that in P3HT:SC blends, the electron mobility in the SC domains is lower than the hole mobility in P3HT, and thus significantly lower than the electron mobility in PCBM.

Even though the photoconductance decay profiles in Figure 4 show that the electrons on different fullerenes have different local mobilities, the data does not allow us to directly make quantitative mobility comparisons between the samples. This is because the overall carrier yield at high fullerene loadings not only depends on the fullerenes' intrinsic ability to split excitons, but also depends on the donor/acceptor interfacial area, which is sensitive to the degree of phase segregation between P3HT and the different fullerenes. Thus, to extract quantitative information about differences in local carrier mobility among the different fullerenes, we need to find a way to determine the carrier yields (φ) in the blend films with different fullerenes. We chose to estimate φ from the degree of fluorescence quenching observed via time-correlated single photon counting (TCSPC). Using the methods outlined in the SI, we excited each of our TRMC samples at 510 nm and monitored the decay of the photoluminescence (PL) at 720 nm, producing the TCSPC data shown in **Figure 5**. After deconvoluting the instrument response function and fitting the resulting PL transients to a sum of two exponentials (see SI), we obtained the PL lifetimes given in Table 2. Presuming that every quenched exciton produces carriers that survive on the TRMC time scale, fluorescence quenching provides a direct measure of the fraction of absorbed excitation photons that produce charge carriers. Unfortunately, not all of the carriers generated through exciton quenching survive to the ns time scales measured in TRMC. We can estimate how many carriers survive to this time scale, however, using our measurements on the dilute fullerene-containing samples. Since all of the measured photoconductance in these samples comes from hole mobility on P3HT, we can use the literature value for P3HT's TRMC hole mobility (0.014 cm^2/Vs[57,59,60]) to calculate φ for each of the different fullerenes on the TRMC time scale. We can then compare this value of φ to that determined from

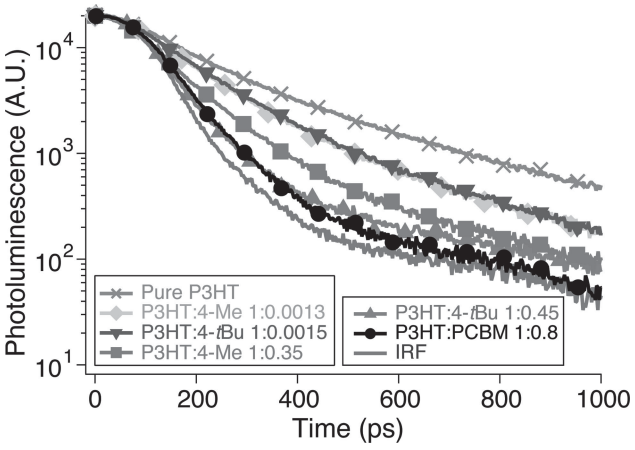

Figure 5. Fluorescence quenching of the polymer:fullerene blend samples used for the TRMC experiments shown in Figure 3 measured by time correlated single photon counting. Symbols have the same meaning as in Figure 3.

Adv. Funct. Mater. **2013**,
DOI: 10.1002/adfm.201301757

our PL quenching measurements to determine the ratio of carriers generated on the ps time scale to those that survive on the ns time scale.

Using this procedure, we were able to determine the local electron mobilities of the 4-Me and 4-*t*Bu SC fullerenes at device-level loadings. Table 2 shows that at high concentrations, the 4-*t*Bu pentaaryl fullerene has a PL lifetime that is shorter than that of the 4-Me molecule, indicating that there is ~30% more PL quenching for P3HT:4-*t*Bu blends than for P3HT:4-Me blends. This result is in excellent agreement with steady-state fluorescence measurements in our previous work, and can be attributed to the enhanced phase separation of the non-stacking 4-Me molecule relative to the self-assembling 4-*t*Bu.[32] Thus, even though the photoconductance of the 4-*t*Bu sample at device loadings is higher than that of the 4-Me sample, most of this difference results from changes in carrier yield. In fact, when we use the information from the dilute samples, we conclude that on the ns time scale of TRMC, the carrier yield for the 4-*t*Bu sample is roughly twice as large as for the 4-Me sample. Since the measured photoconductance for these two samples also differs by a factor of two, this means that the local mobilities of these two SC fullerenes must be roughly similar, in accord with the DFT calculations presented in the previous section. This also implies that the dramatic differences in device performance observed between BHJs with these two fullerenes[32] must result from differences in the macroscopic mobility of the fullerene network, verifying that the self-assembling 4-*t*Bu molecule forms a significantly better interpenetrating network than its non-assembling 4-Me analogue.

Also of interest in Figure 3 and Table 2 is the fact that the PL lifetimes of P3HT:4-*t*Bu and P3HT:PCBM[57] blends at device loadings (high weight ratios) are essentially identical, resulting in fairly similar carrier yields on the ps time scale of the TCSPC measurement. If we continue to assume that the hole mobility of P3HT does not change when increasing fullerene loading, then the difference in the TRMC-measured $\varphi\Sigma\mu = \varphi(\mu_e + \mu_h)$ product at higher fullerene loadings are caused both by a decreased φ and a decreased local electron mobility for the SCs relative to PCBM. We note that the value for the local electron mobility that we extract for PCBM at the 1:0.8 blend ratio is somewhat lower than previously reported,[57] which is caused by the different processing conditions used here. Our analysis confirms, however, that the local electron mobility in PCBM is at least a factor of five higher than that in 4-*t*Bu, as summarized in Table 2. This is also consistent with our DFT calculations in the previous section, and verifies that the reason PCBM is such a good electron acceptor for use in polymer blend solar cells is because it has outstanding local mobility due to the strong overlap of the LUMOs between adjacent molecules, even though it doesn't necessarily form the best macroscopic BHJ network.

Finally, to examine how the macroscopic fullerene network changes with the different SCs molecules, we constructed diodes out of films of the pure 4-*t*Bu and 4-Me molecules; the details of the fabrication and construction of these fullerene-only diodes are given in the SI. We fit the measured current-voltage curves for these SC diodes to the Mott-Gurney law, and extracted the space-charge limited macroscopic electron mobilities for these fullerenes of 3.9 and 0.7×10^{-6} cm^2/Vs for 4-*t*Bu and 4-Me, respectively. Since the local electron mobilities of these two fullerenes are similar to each other (0.49 and 0.44×10^{-2} cm^2/Vs), this result verifies that the nature of the electron-conducting network is also important for macroscopic mobility/overall charge extraction. Although carriers may be able to move with similar ease between adjacent 4-*t*Bu and 4-Me fullerene molecules, the global network formed with the 4-*t*Bu fullerene is more than five times more effective at moving charges across macroscopic distances than the network formed by 4-Me fullerenes. It is important to emphasize that this conclusion was based on diodes fabricated from pure fullerene films, so the data is influenced only by the macroscopic connectivity of the fullerene network and not by polymer/fullerene phase separation. For comparison, it is worth noting that the space-charge limited electron mobility of both SC fullerenes is much lower than that of PCBM (2.0×10^{-4} cm^2/Vs[61]). Thus, as we have argued throughout this work, both network formation and good local electronic coupling are important to obtain efficient charge extraction from an organic photovoltaic device.

3. Conclusions

In this paper, we have used both theoretical and experimental techniques to better understand the distinction between the local mobility and the macroscopic mobility of electrons on the fullerene network of polymer-based BHJ photovoltaic devices. Our work shows that there are indeed two significant components to electron mobility: the intrinsic ability of electrons to move between adjacent fullerenes (local mobility), and the overall architecture and morphology of the fullerene network on device length scales (macroscopic mobility). The macroscopic mobility is what is typically measured in device physics experiments, and we have shown that a good understanding of local mobility can be obtained from a combination of DFT calculations and TRMC experimental measurements.

To understand the differences between local and macroscopic mobility, we examined the behavior of BHJ blends of P3HT and a pair of pentaaryl fullerene derivatives that have an identical electronic structure but different propensities to self-assemble on macroscopic length scales. Our DFT calculations found that the coupling between adjacent molecules is quite similar for the self-assembling 4-*t*Bu and non-assembling 4-Me shuttlecock fullerenes, so that with their nearly identical electronic structure, their local electron mobilities are also nearly identical. Our TRMC experiments on blends of these fullerenes show that the local electron mobilities on these are indeed comparable; the slightly higher net local mobility for the 4-*t*Bu molecule is likely directly related to the fact that self-assembly can assist mobility even on the local length scales probed by TRMC. More importantly, however, photovoltaic devices fabricated with 4-*t*Bu show dramatically better performance than those fabricated with 4-Me[32] and diodes built from 4-*t*Bu have a higher space-charge limited mobility than those built from 4-Me, verifying that changes in the macroscopic network morphology affect device performance even when the local mobilities are comparable.

We also used the idea of separate local and macroscopic electron mobilities to understand why PCBM is the fullerene

of choice for nearly every polymer-based photovoltaic. Our DFT calculations show that the local electronic behavior of PCBM is nearly ideal for solar cells: the coupling between adjacent molecules is very high, and the delocalization of the frontier orbitals allows for efficient charge transfer in almost every orientation. This is in contrast to the SC fullerenes, whose frontier orbitals are perturbed by the presence of the pentaadducts, leading to poorer electronic overlap. Our TRMC experiments verified that the local electron mobility on PCBM is significantly higher than that on the SC fullerenes, consistent with the fact that PCBM consistently produces the best photovoltaic devices.

Finally, all of our results suggest that there is further room for improvement in the fullerene component of polymer BHJ solar cells. Since self-assembly can produce macroscopic networks that dramatically improve device performance, it seems clear that designing new fullerenes that both self-assemble and have high local electron mobilities should produce devices that are even better than those using PCBM, particularly since it has been argued that electron mobility on the fullerene network is what limits overall device performance.[62] Furthermore PCBM has a low LUMO compared to novel fullerene acceptors like ICBA.[63,64] Future fullerene acceptors that utilize self-assembly and possess a higher lying LUMO will potentially lead to improvements in both open circuit voltage and short circuit current. The fact that our DFT calculations are corroborated by experiment means that we can design new fullerenes and test them for local mobility before synthesizing them. In combination with TRMC and other measurements, this should provide a way to explore new self-assembling fullerenes that are simultaneously optimized for both local and macroscopic electron mobility, thus helping polymer-based photovoltaic devices to reach their ultimate potential.

Acknowledgements

A portion of the research was performed using the computing resources at EMSL, a national scientific user facility sponsored by the US Department of Energy (DOE) Office of Biological and Environmental Research and located at Pacific Northwest National Laboratory (PNNL). PNNL is operated for the DOE by the Battelle Memorial Institute under contract DE-AC06-76RLO-1830. The work of the UCLA and NREL members was supported as part of the Molecularly Engineered Energy Materials (MEEM), an Energy Frontier Research Center funded by the US Department of Energy, Office of Science, Office of Basic Energy Sciences under Award Number DE-SC0001342. J.C.A. acknowledges NSF IGERT: Materials Creation Training Program (MCTP), grant number DGE-0654431 and the California NanoSystems Institute. Support for the synthesis of the shuttlecock molecules was provided by the National Science Foundation under grant CHE-1112569.

Received: May 22, 2013
Revised: June 18, 2013
Published online:

[1] G. Yu, J. Gao, J. C. Hummelen, F. Wudl, A. J. Heeger, *Science* **1995**, *270*, pp. 1789.
[2] A. A. Bakulin, A. Rao, V. G. Pavelyev, P. H. M. van Loosdrecht, M. S. Pshenichnikov, D. Niedzialek, J. Cornil, D. Beljonne, R. H. Friend, *Science* **2012**, *335*, 1340.
[3] K. Li, P. P. Khlyabich, L. Li, B. Burkhart, B. C. Thompson, J. C. Campbell, *J. Phys. Chem. C* **2013**, *117*, 6940.
[4] P. E. Keivanidis, T. M. Clarke, S. Lilliu, T. Agostinelli, J. E. Macdonald, J. R. Durrant, D. D. C. Bradley, J. Nelson, *J. Phys. Chem. Lett.* **2010**, *1*, 734.
[5] S. R. Forrest, *MRS Bull.* **2005**, *30*, 28.
[6] B. M. Savoie, S. Tan, J. Jerome, C. W. Shu, M. Ratner, T. Marks, *"Ascertaining the limitations of low mobility on organic solar cell performance"*, 15th International Workshop on Computational Electronics (IWCE), **22–25 May 2012**
[7] J. D. Kotlarski, D. J. D. Moet, P. W. M. Blom, *J. Polym. Sci. B: Polym. Phys.* **2011**, *49*, 708.
[8] B. Tremolet de Villers, C. J. Tassone, S. H. Tolbert, B. J. Schwartz, *J. Phys. Chem. C* **2009**, *113*, 18978.
[9] S. Jeong, Y. Kwon, B. D. Choi, H. Ade, Y. S. Han, *Appl. Phys. Lett.* **2010**, *96*, 183305–183305.
[10] F. Etzold, I. A. Howard, R. Mauer, M. Meister, T. D. Kim, K. S. Lee, N. S. Baek, F. Laquai, *J. Am. Chem. Soc.* **2011**, *133*, 9469.
[11] C. Bruner, N. C. Miller, M. D. McGehee, R. H. Dauskardt, *Adv. Funct. Mater.* **2013**, *23*, 2863.
[12] H. Hoppe, N. S. Sariciftci, *J. Mater. Chem.* **2006**, *16*, 45.
[13] H. Yan, B. A. Collins, E. Gann, C. Wang, H. Ade, C. R. McNeill, *ACS Nano* **2011**, *6*, 677.
[14] W. L. Rance, A. J. Ferguson, T. McCarthy-Ward, M. Heeney, D. S. Ginley, D. C. Olson, G. Rumbles, N. Kopidakis, *ACS Nano* **2011**, *5*, 5635.
[15] P. A. Troshin, H. Hoppe, J. Renz, M. Egginger, J. Y. Mayorova, A. E. Goryachev, A. S. Peregudov, R. N. Lyubovskaya, G. Gobsch, N. S. Sariciftci, V. F. Razumov, *Adv. Funct. Mater.* **2009**, *19*, 779.
[16] Y. Liang, L. Yu, *Acc. Chem. Res.* **2010**, *43*, 1227.
[17] J. Peet, C. Soci, R. C. Coffin, T. Q. Nguyen, A. Mikhailovsky, D. Moses, G. C. Bazan, *Appl. Phys. Lett.* **2006**, *89*, 252105.
[18] J. Peet, J. Y. Kim, N. E. Coates, W. L. Ma, D. Moses, A. J. Heeger, G. C. Bazan, *Nat. Mater.* **2007**, *6*, 497.
[19] J. K. Lee, W. L. Ma, C. J. Brabec, J. Yuen, J. S. Moon, J. Y. Kim, K. Lee, G. C. Bazan, A. J. Heeger, *J. Am. Chem. Soc.* **2008**, *130*, 3619.
[20] W. Ma, C. Yang, X. Gong, K. Lee, A. Heeger, *Adv. Funct. Mater.* **2005**, *15*, 1617.
[21] K. Kim, J. Liu, M. A. G. Namboothiry, D. L. Carroll, *Appl. Phys. Lett.* **2007**, *90*, 163511.
[22] E. Verploegen, R. Mondal, C. J. Bettinger, S. Sok, M. F. Toney, Z. Bao, *Adv. Funct. Mater.* **2010**, *20*, 3519.
[23] A. L. Ayzner, C. J. Tassone, S. H. Tolbert, B. J. Schwartz, *J. Phys. Chem. C* **2009**, *113*, 20050.
[24] A. M. Nardes, A. L. Ayzner, S. R. Hammond, A. J. Ferguson, B. J. Schwartz, N. Kopidakis, *J. Phys. Chem. C* **2012**, *116*, 7293.
[25] A. L. Ayzner, S. C. Doan, B. Tremolet, de Villers, B. J. Schwartz, *J. Phys. Chem. Lett.* **2012**, *3*, 2281.
[26] C. Tao, M. Aljada, P. E. Shaw, K. H. Lee, H. Cavaye, M. N. Balfour, R. J. Borthwick, M. James, P. L. Burn, I. R. Gentle, P. Meredith, *Adv. Energy Mater.* **2013**, *3*, 105.
[27] D. H. Wang, J. S. Moon, J. Seifter, J. Jo, J. H. Park, O. O. Park, A. J. Heeger, *Nano Lett.* **2011**, *11*, 3163.
[28] H. Li, Y. F. Li, J. Wang, *Appl. Phys. Lett.* **2012**, *101*, 033907.
[29] C. W. Rochester, S. A. Mauger, A. J. Moulé, *J. Phys. Chem. C* **2012**, *116*, 7287.
[30] A. Loiudice, A. Rizzo, M. Biasiucci, G. Gigli, *J. Phys. Chem. Lett.* **2012**, *3*, 1908.
[31] R. D. Kennedy, A. L. Ayzner, D. D. Wanger, C. T. Day, M. Halim, S. I. Khan, S. H. Tolbert, B. J. Schwartz, Y. Rubin, *J. Am. Chem. Soc.* **2008**, *130*, 17290.
[32] C. J. Tassone, A. L. Ayzner, R. D. Kennedy, M. Halim, M. So, Y. Rubin, S. H. Tolbert, B. J. Schwartz, *J. Phys. Chem. C* **2011**, *115*, 22563.

[33] R. D. Kennedy, M. Halim, S. I. Khan, B. J. Schwartz, S. H. Tolbert, Y. Rubin, *Chem. Eur. J.* **2012**, *18*, 7418.
[34] M. Sawamura, K. Kawai, Y. Matsuo, K. Kanie, T. Kato, E. Nakamura, *Nature* **2002**, *419*, 702.
[35] K. Huebener, M. Scheloske, J. Hauschild, W. Harneit, G. Zehl, S. Fiechter, *Phys. Status Solidi B* **2006**, *243*, 2990.
[36] S. Okada, R. Arita, Y. Matsuo, E. Nakamura, A. Oshiyama, H. Aoki, *Chem. Phys. Lett.* **2004**, *399*, 157.
[37] V. Bashilov, F. Dolgushin, B. Tumanskii, P. Petrovskii, V. Sokolov, *Tetrahedron* **2008**, *64*, 11291.
[38] M. T. Rispens, A. Meetsma, R. Rittberger, C. J. Brabec, N. S. Sariciftci, J. C. Hummelen, *Chem. Commun.* **2003**, 2116.
[39] R. A. Marcus, N. Sutin, *Biochim. Biophys. Acta* **1985**, *811*, 265.
[40] J. Kirkpatrick, *Int. J. Quantum Chem.* **2008**, *108*, 51.
[41] J. L. Brédas,D. Beljonne, V. Coropceanu, J. Cornil, *Chem. Rev.* **2004**, *104*, 4971.
[42] V. Lemaur, D. A. da Silva Filho, V. Coropceanu, M. Lehmann, Y. Geerts, J. Piris, M. G. Debije, A. M. van de Craats, K. Senthilkumar, L. D. A. Siebbeles, J. M. Warman, J. L. Brédas, J. Cornil, *J. Am. Chem. Soc.* **2004**, *126*, 3271.
[43] Q. Wu, T. V. Voorhis, *J. Chem. Phys.* **2006**, *125*, 164105.
[44] T. Stein, L. Kronik, R. Baer, *J. Am. Chem. Soc.* **2009**, *131*, 2818.
[45] C. Liu, D. Walter, D. Neuhauser, R. Baer, *J. Am. Chem. Soc.* **2003**, *125*, 13936.
[46] H. Chen, M. A. Ratner, G. C. Schatz, *J. Phys. Chem. C* **2011**, *115*, 18810.
[47] M. Raja, G. C. R. Lloyd, N. Sedghi, W. Eccleston, R. Di Lucrezia, S. J. Higgins, *J. Appl. Phys.* **2002**, *92*, 1441.
[48] W. Geens, T. Martens, J. Poortmans, T. Aernouts, J. Manca, L. Lutsen, P. Heremans, S. Borghs, R. Mertens, D. Vanderzande, *Thin Solid Films* **2004**, *451–452*, 498, Proceedings of Symposium D on Thin Film and Nano-Structured Materials for Photovoltaics, of the E-MRS 2003 Spring Conference.
[49] S. Choulis, J. Nelson, Y. Kim, D. Poplavskyy, T. Kreouzis, J. Durrant, D. D. C. Bradley, *Appl. Phys. Lett.* **2003**, *83*, 3812.
[50] G. Juška, K. Arlauskas, M. Vili nas, J. Ko ka, *Phys. Rev. Lett.* **2000**, *84*, 4946.
[51] A. Mozer, N. Sariciftci, L. Lutsen, D. Vanderzande, R. Osterbacka, M. Westerling, G. Juska, *Appl. Phys. Lett.* **2005**, *86*, 112104.
[52] C. G. Shuttle, R. Hamilton, J. Nelson, B. C. O'Regan, J. R. Durrant, *Adv. Funct. Mater.* **2010**, *20*, 698.
[53] G. Dicker, M. P. de Haas, L. D. Siebbeles, J. M. Warman, *Phys. Rev. B* **2004**, *70*, 045203.
[54] A. J. Ferguson, J. L. Blackburn, J. M. Holt, N. Kopidakis, R. C. Tenent, T. M. Barnes, M. J. Heben, G. Rumbles, *J. Phys. Chem. Lett.* **2010**, *1*, 2406.
[55] P. Pingel, A. Zen, R. D. Abellón, F. C. Grozema, L. D. Siebbeles, D. Neher, *Adv. Funct. Mater.* **2010**, *20*, 2286.
[56] A. J. Ferguson, N. Kopidakis, S. E. Shaheen, G. Rumbles, *J. Phys. Chem. C* **2008**, *112*, 9865.
[57] A. J. Ferguson, N. Kopidakis, S. E. Shaheen, G. Rumbles, *J. Phys. Chem. C* **2011**, *115*, 23134.
[58] W. J. Grzegorczyk, T. J. Savenije, T. E. Dykstra, J. Piris, J. M. Schins, L. D. Siebbeles, *J. Phys. Chem. C* **2010**, *114*, 5182.
[59] G. Dicker, M. P. de Haas, J. M. Warman, D. M. de Leeuw, L. D. A. Siebbeles, *J. Phys. Chem. B* **2004**, *108*, 17818.
[60] O. G. Reid, J. A. N. Malik, G. Latini, S. Dayal, N. Kopidakis, C. Silva, N. Stingelin, G. Rumbles, *J. Polym. Sci. B Polym. Phys.* **2012**, *50*, 27.
[61] V. Mihailetchi, J. van Duren, P. Blom, J. Hummelen, R. Janssen, J. Kroon, M. Rispens, W. Verhees, M. Wienk, *Adv. Funct. Mater.* **2003**, *13*, 43.
[62] A. L. Ayzner, D. D. Wanger, C. J. Tassone, S. H. Tolbert, B. J. Schwartz, *J. Phys. Chem. C* **2008**, *112*, 18711.
[63] Y. He, H. Y. Chen, J. Hou, Y. Li, *J. Am. Chem. Soc.* **2010**, *132*, 1377.
[64] G. Zhao, Y. He, Y. Li, *Adv. Mater.* **2010**, *22*, 4355.